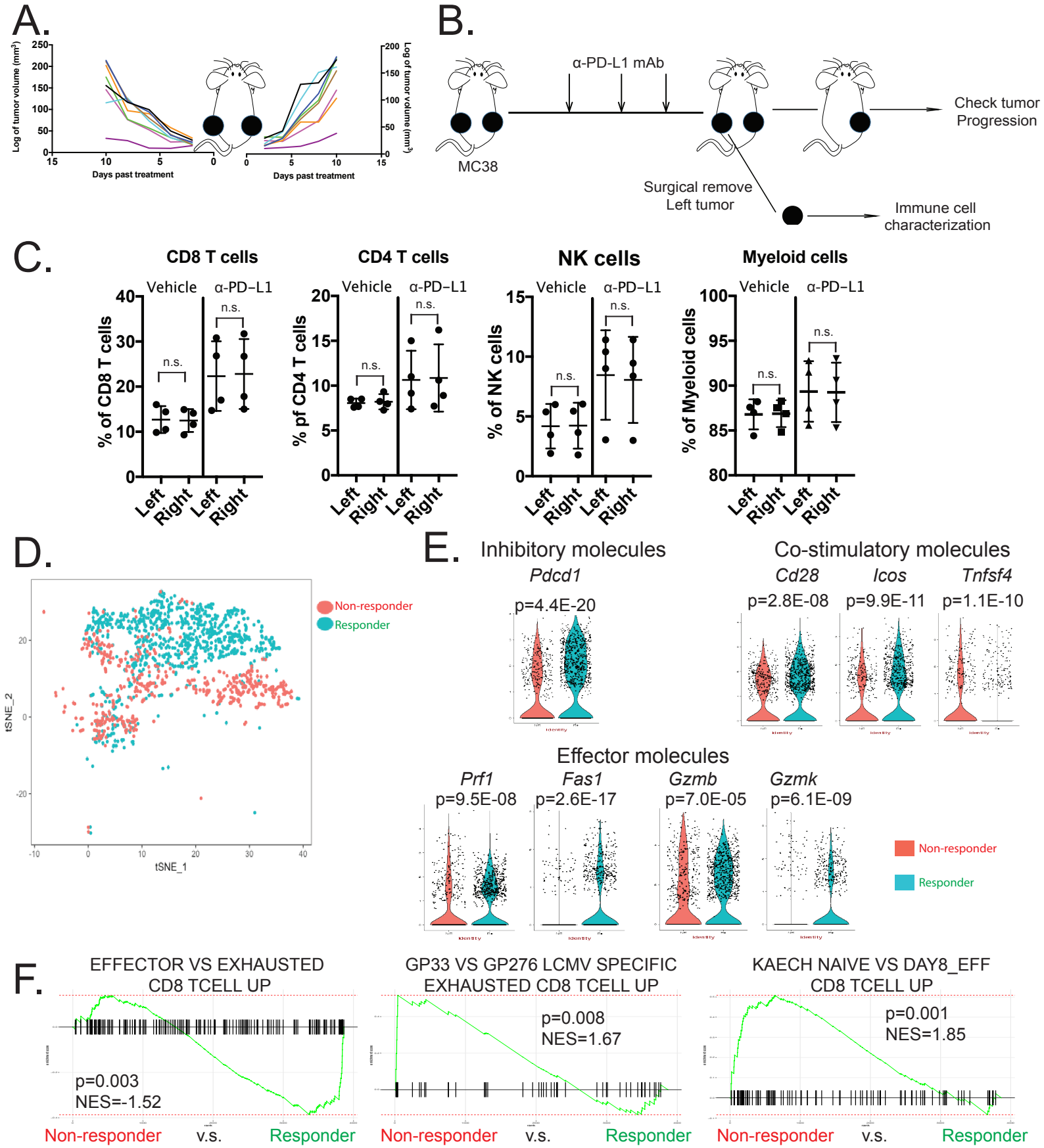

Supplemental Figure 1. Schema of bilateral tumor models and enrichment of dysfunctional tumor infiltrating CD8 T cells in non-responder to α-PD-L1 mAb.

(A) Representative growth curve shows the individual tumor progression of mice with bilateral MC38 tumors treated with vehicle (n = 4) and α-PD-L1 mAb (n = 4), color-coded per mouse. (B) Schedule of experimental design. (C) The frequency of CD8 T cells, CD4 T cells, NK cells and CD11b^{+} myeloid cells inside tumors from different treatment groups. (D) t-Distributed Stochastic Neighbor Embedding (t-SNE) plot demonstrates CD8 T cell clusters from tumors responding and resistant to α-PD-L1 treatment. (E) Violin plots show the gene expression probability distribution of inhibitory molecules, co-stimulatory molecules and effector molecules in CD8 T cell clusters. (F) GSEA plots reveal the negative enrichment of effector CD8 T cell signature and positive enrichment of exhausted and naïve CD8 T cell signatures in CD8 T cells from non-responsive versus responsive tumors.

Supplemental Figure 1

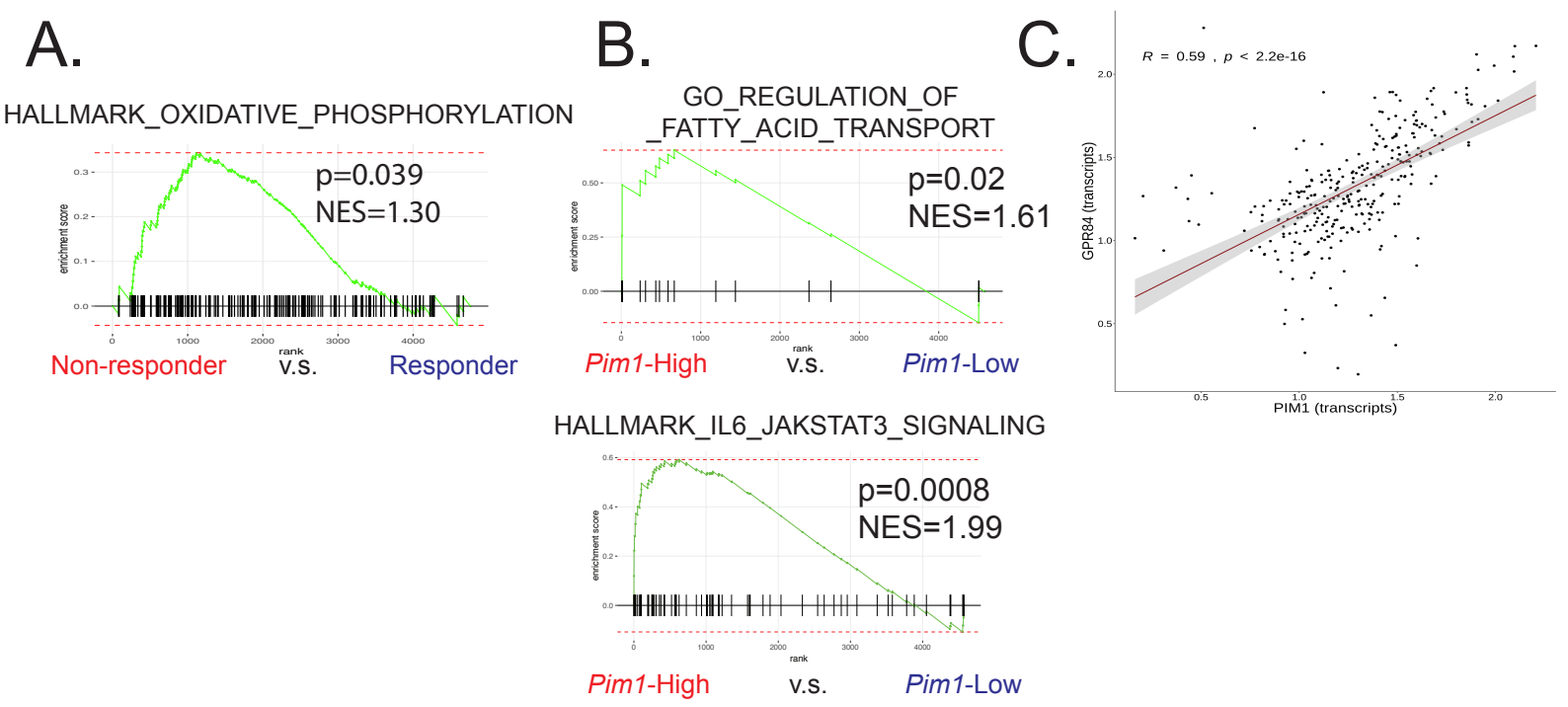

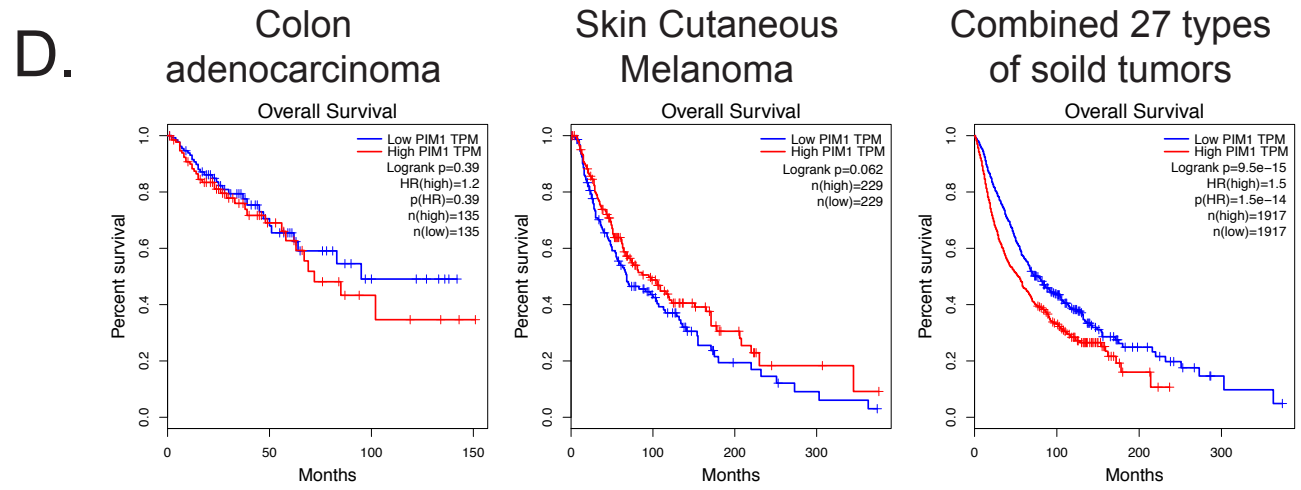

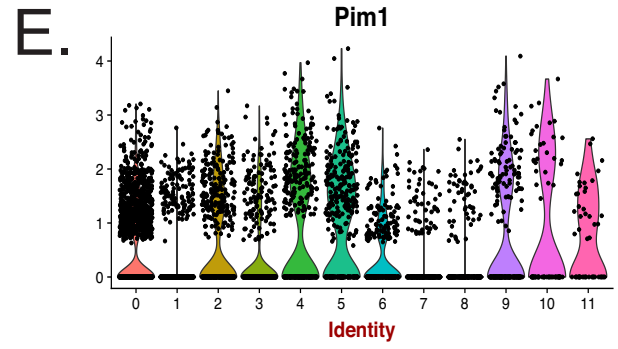

Supplemental Figure 2. The correlation of PIM1 with fatty acid metabolism in myeloid cells and the clinical relevance of PIM1 expression in resistance to immune checkpoint blockade (ICB).
(A) GSEA plots show the enrichment of oxidative phosphorylation signatures in myeloid cells from responsive versus nonresponsive tumors. (B) GSEA plots show the enrichment of fatty acid transport and IL-6/-JAK/STAT3 signaling signatures in Pim1^{high} myeloid cells versus Pim1^{low} myeloid cells. (C) The expression of *GPR84* was correlated with *PIM1* in tumor infiltrating myeloid cells from melanoma patient scRNA-seq data. (D) Kaplan-Meier survival curves of patients with solid tumors containing high levels of PIM1 versus those with low levels of PIM1 were generated from GEPIA(http://gepia.cancer-pku.cn) (E) Violin plots show the expression of *Pim1* in mouse bearing MC38 tumor treated with α-PD-L1 mAb

Supplemental Figure 2

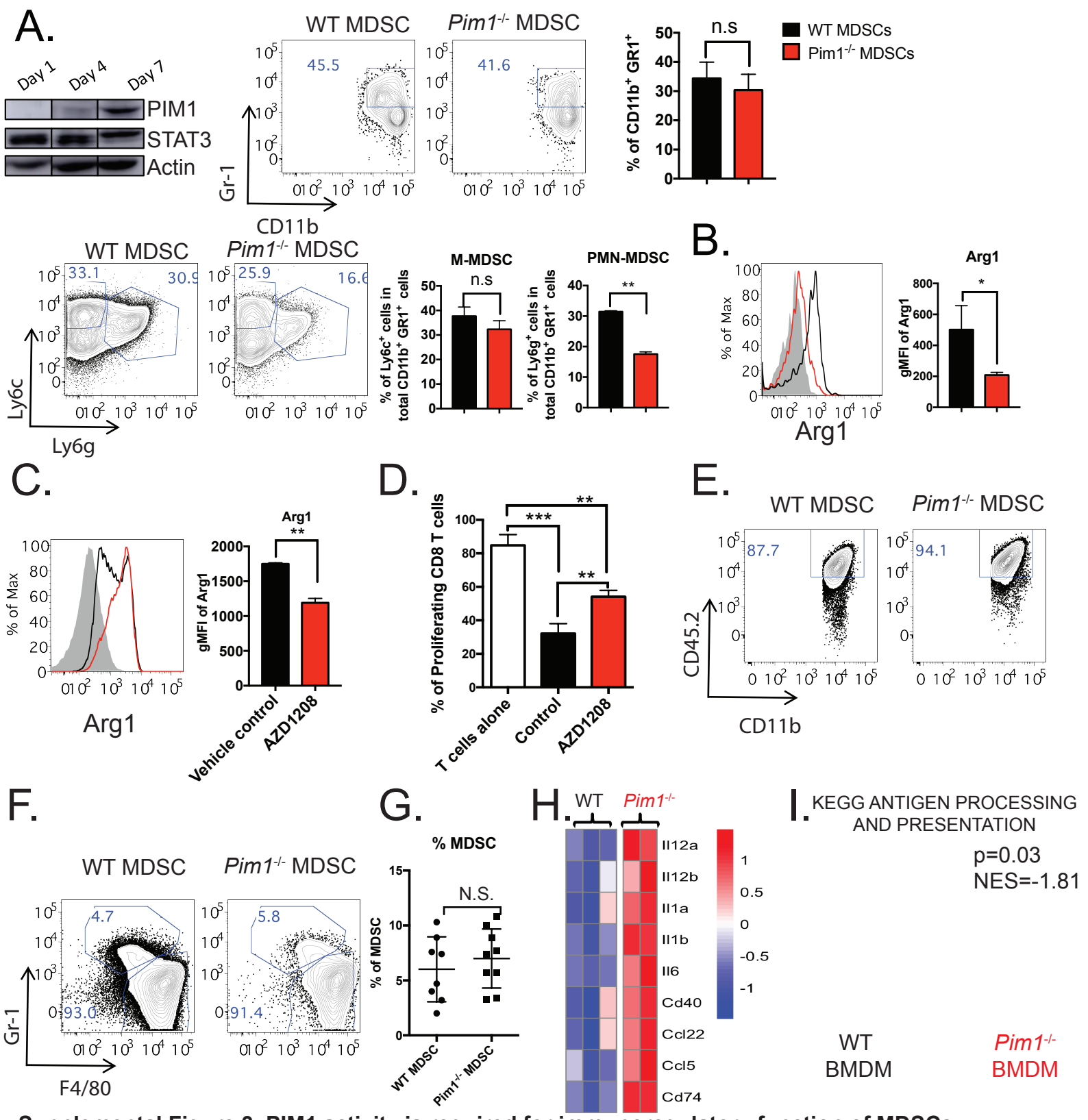

Supplemental Figure 3. PIM1 activity is required for immunoregulatory function of MDSCs.
(A) Immunoblot analysis of PIM1 expression in BM-MDSCs (Top) and flow cytometry analysis of total CD11b+Gr1+; Ly6g+CD11b+Gr1+ and Ly6c+CD11b+Gr1+ cells between WT and *Pim1*$^{-/-}$ BM-MDSCs. (B-C) The protein level of Arg1 was measured by flow cytometry in either genetic deletion (B) or pharmacological inhibition (C) of PIM1. (D) The immunosuppressive function affected by AZD1208 treatment was assayed by measuring the ability of MDSCs to inhibit the proliferation of activated T cells. Data are expressed as mean ± SEM from two experiments. (E) Representative flow cytometry plots show the proportion of transferred WT and *Pim1*$^{-/-}$ BM-MDSCs from tumor. (F-G) Flow cytometric analysis and quantification of tumor-infiltrating myeloid cells by measuring the expression of Gr1 (MDSCs) and F4/80 (macrophages) in CD11b^{+} cell populations. The histogram bars show the percentage of Gr1^{+} cells in total in CD11b^{+} cells. (H) Heatmap shows the expression of genes associated with M1 inflammatory macrophages in BMDM generated from WT and *Pim1*$^{-/-}$ mice.(I) GSEA analysis demonstrating that Pim1-/- BMDM exhibited enriched gene signatures related to antigen processing and presentation. *p < 0.05, **p < 0.01.

Supplemental Figure 3

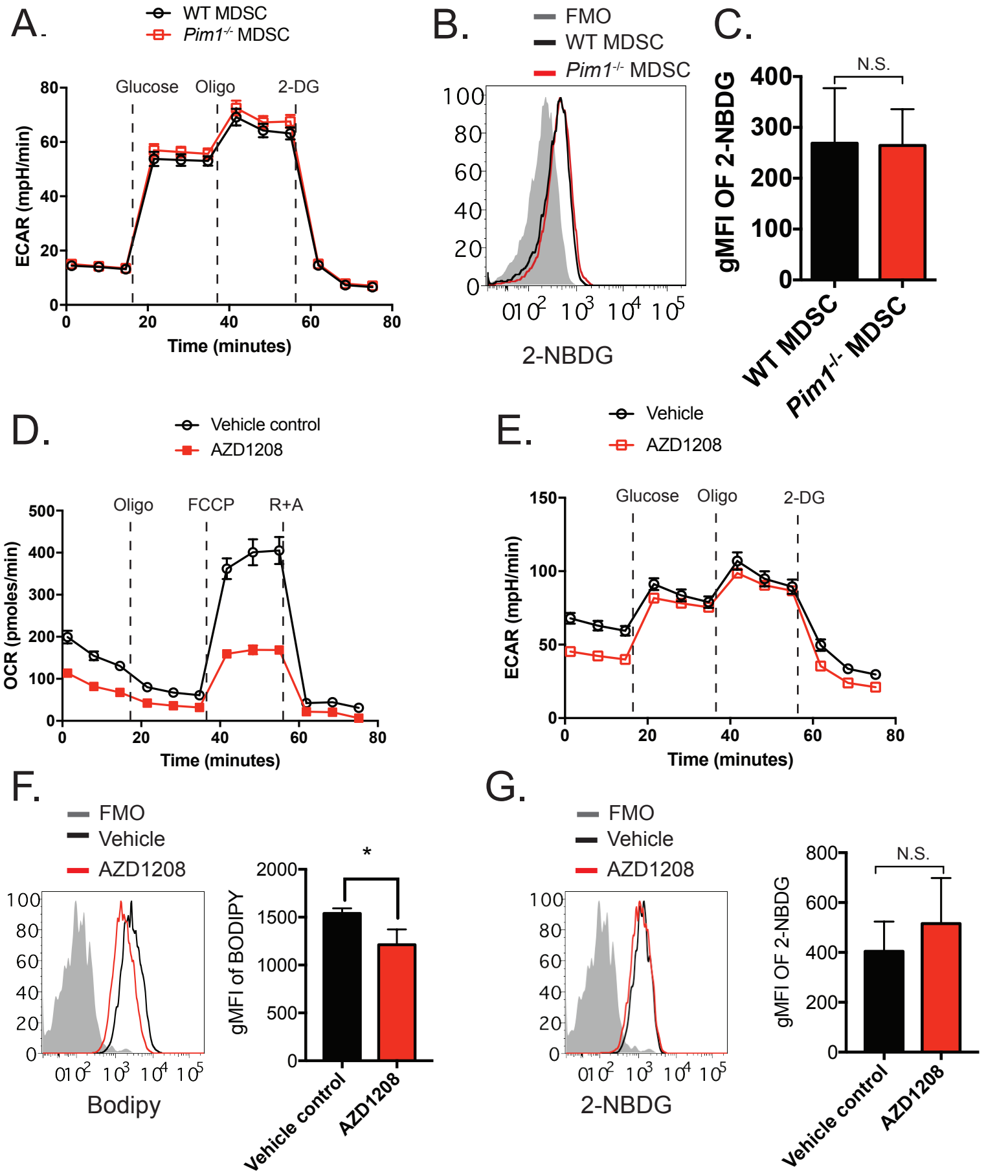

Supplemental Figure 4. Genetic deletion or pharmacologic inhibition of PIM1 reduces fatty acid metabolism in MDSCs.

(A) The representative graph shows the extracellular acidification rate (ECAR) measured in WT and *Pim1*$^{-/-}$ MDSCs. (B-C) Uptake of 2-NBDG was measured by flow cytometry (B), and the results were quantified (C). (D-G) WT MDSCs were treated with AZD1208 over 7 days to inhibit PIM1. The effect of AZD1208 on cellular respiration was measured by oxygen consumption rate (OCR) and shown in Figure D, while its effect on glycolysis was examined by ECAR (E). The uptake of fatty acids (F) and and 2-NBDG (G) were also measured by flow cytometry. *$p < 0.05$. FMO = Fluorescence Minus One.

Supplemental Figure 4

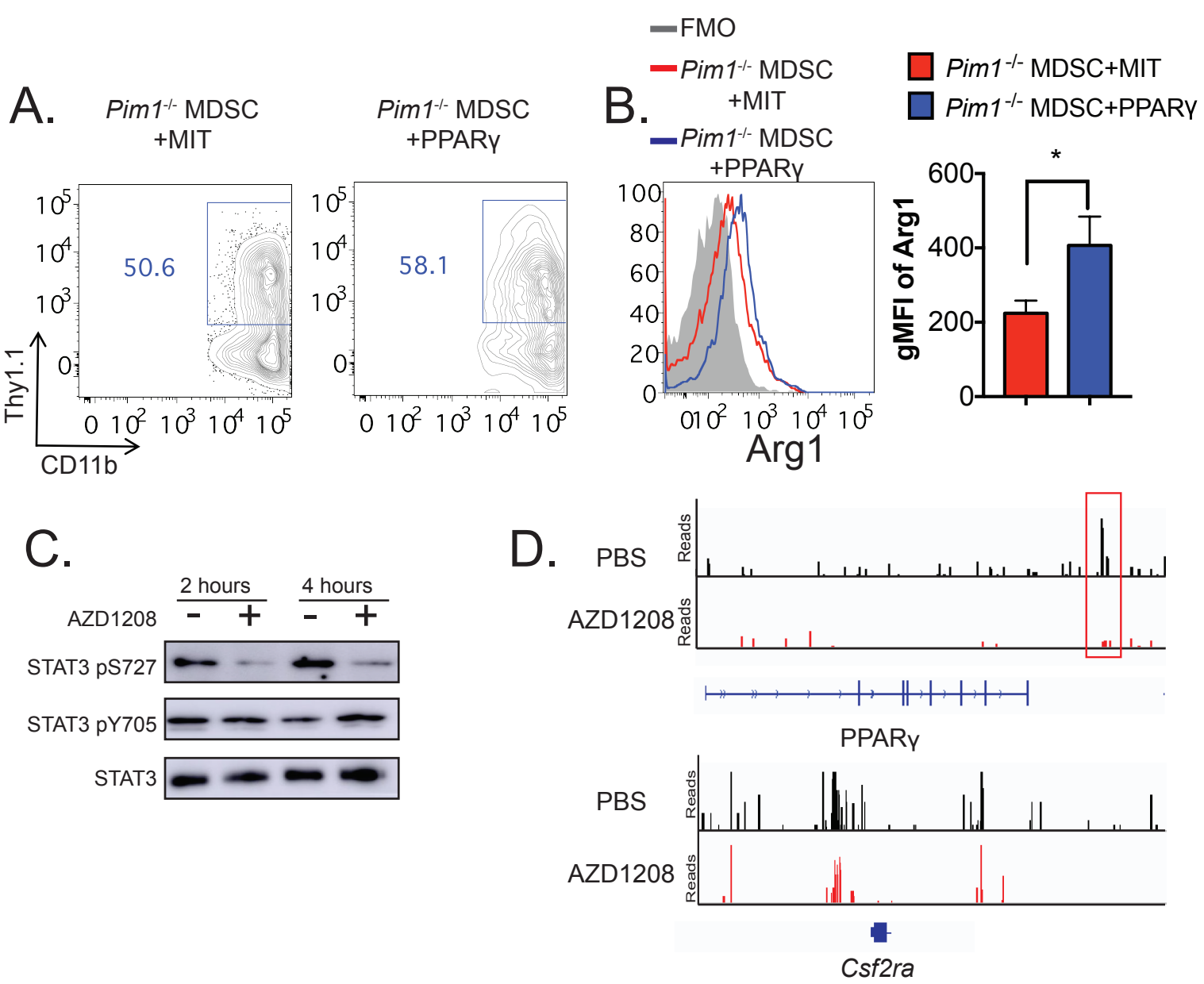

Supplemental Figure 5. Overexpression of PPARγ rescues the expression of Arg1 in Pim1$^{-/-}$ MDSCs. A) The percentage of positively transduced cells were monitored by Thy1.1 expression. (B) Protein levels of Arg1 were assessed in PPARγ-overexpressing *Pim1*$^{-/-}$ MDSCs by flow cytometry and the results were quantified. *p < 0.05. FMO = Fluorescence Minus One. (C) Western blot analysis of total STAT3, STAT3Ser727, and STAT3Y705 in untreated and AZD1208 treated BM-MDSCs. (D) CUT&Tag chromatin profiling showing STAT3 binding to the *Pparg* and *Csf2ra* loci in BM-MDSCs treated with PBS (top) and AZD1208 (bottom). Data are expressed as mean ±SEM from two experiments. *p < 0.05.

Supplemental Figure 5

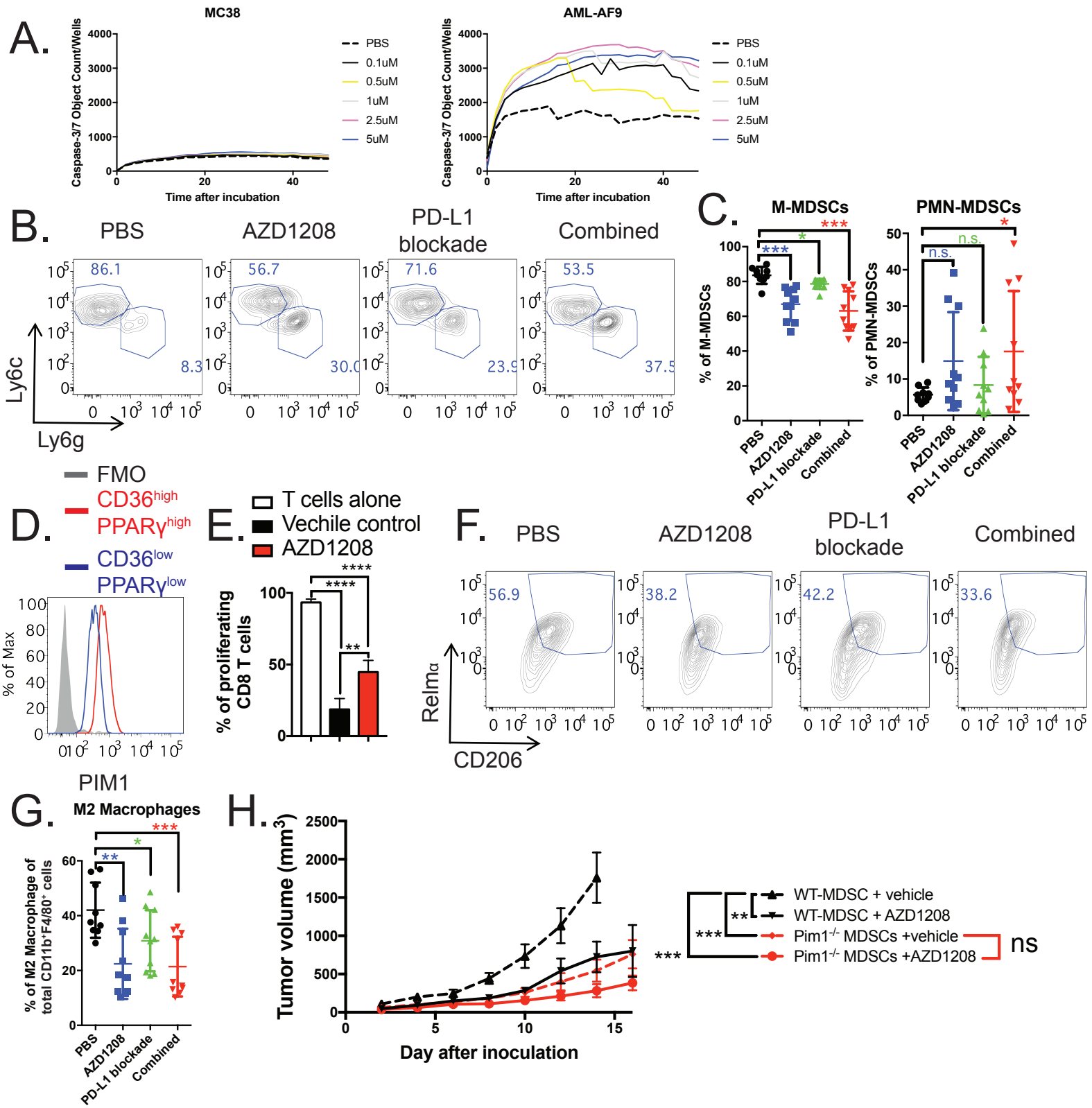

Supplemental Figure 6. Treatment with AZD1208 produces immune-related antitumor efficacy in the MC38 tumor model.

(A) The effect of AZD1208 on inducing apoptosis in MC38 and AML-AF9 cells was determined by staining with caspase 3/7 and measured in real-time by IncuCyte Zoom live-cell imaging system. (B-G) C57BL/6 mice received the therapy regimen described in Figure 6. The percentage of $Ly6c^+$ M-MDSCs and $Ly6g^+$ PMN MDSCs in total $CD11b^+Gr1^+$ cells is shown in representative plots (B) and quantified (C). The expression of PIM1 was compared between $CD36^{high}PPAR\gamma^{high}$ and $CD36^{low}PPAR\gamma^{low}$ cells and shown in D. The $Gr1^+CD11b^+$ cells were isolated from MC38 tumor treated with either vehicle or AZD1208. Then these cells were co-cultured with activated CD8 T cells for suppression assay and quantified in E. The percentage of $CD206^+Relm\alpha^+$ M2 macrophages in total $CD11b^+F4/80^+$ cells is shown in representative plots (F) and quantified (G). (H) WT or *Pim1*$^{-/-}$ BM-MDSCs were adoptively transferred into MC38 tumor bearing mice and treated them as following: 1) WT MDSCs + vehicle control; 2) *Pim1*$^{-/-}$ MDSCs + Vehicle control; 3) WT MDSCs + AZD1208; 4) *Pim1*$^{-/-}$ MDSCs + AZD1208. Tumor growth was monitored in all groups. *p < 0.05, **p < 0.01, ***p < 0.001. FMO = Fluorescence Minus One.

Supplemental Figure 6

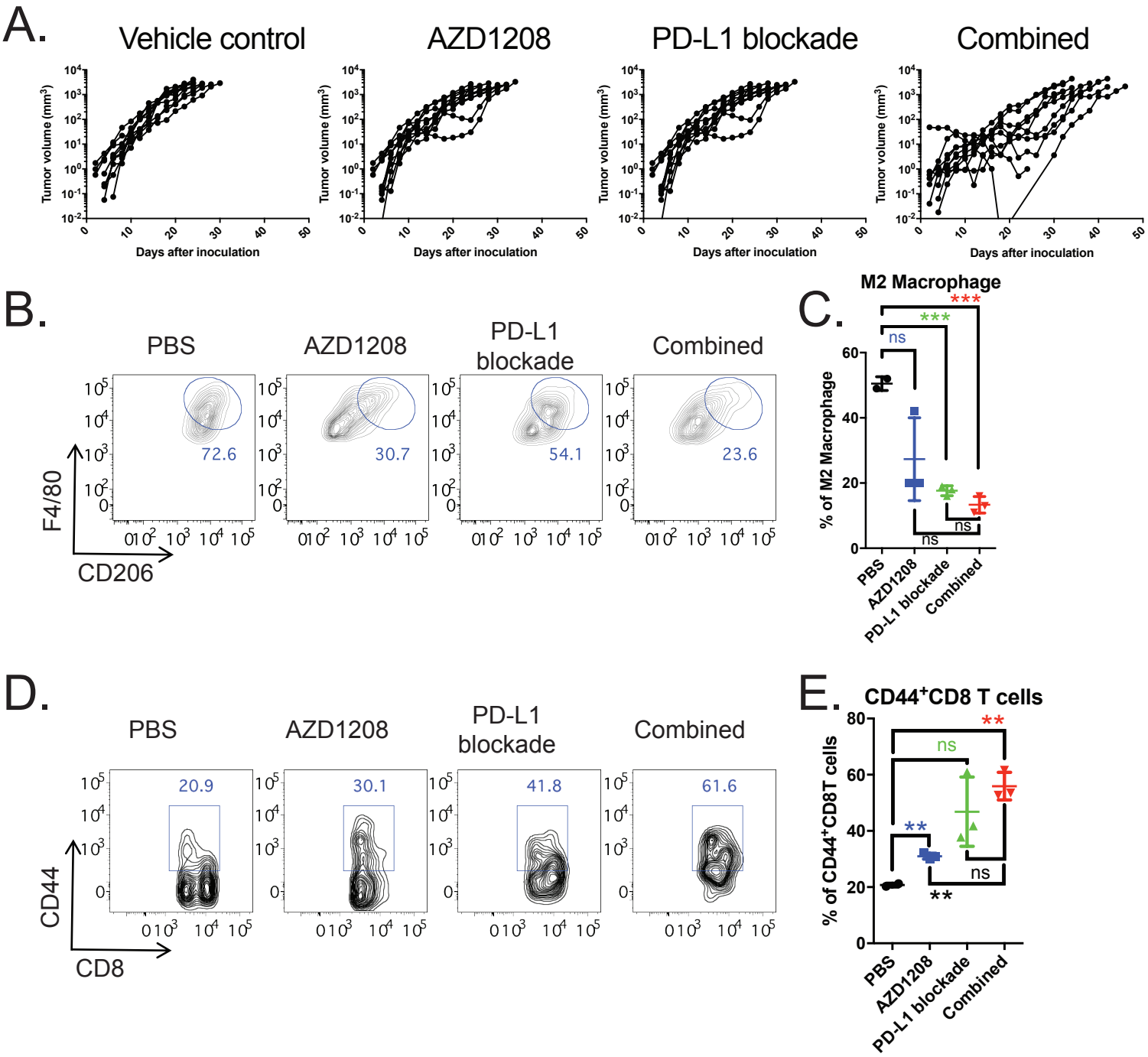

Supplemental Figure 7. AZD120 treatment increase efficacy of α-PD-L1 mAb in B16-BL6 tumor model. (A) C57BL/6 mice were inoculated with B16-BL6 tumor and treated with B16-GM-CSF vaccination (Gvax). In addition to Gvax, these mice were treated with following additional regimens: 1) vehicle, 2) AZD1208, 3) α-PD-L1 mAb, 4) α-PD-L1 mAb in combination with AZD1208. The tumor growth in all four groups was monitored. (B-C) The percentage of $CD206^{+}F4/80^{+}$ M2 macrophages in total $CD11b^{+}F4/80^{+}$ cells are shown in representative plots and quantitative scatter plots. (D-E) The percentage of $CD44^{+}CD8^{+}$ cells in are shown in representative plots and quantitative scatter plots. $^{**}p < 0.01$, $^{***}p < 0.001$.

Supplemental Figure 7

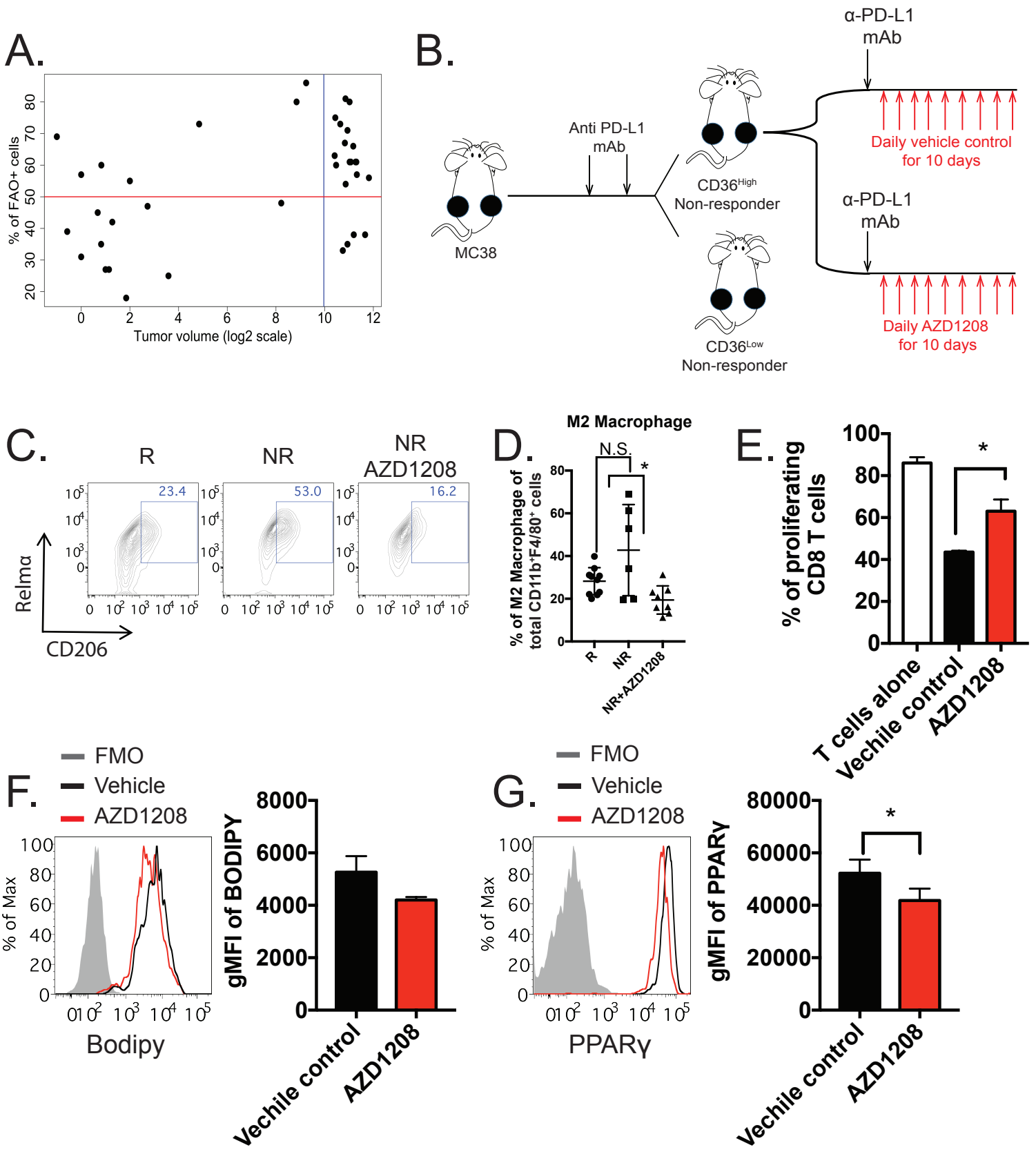

Supplemental Figure 8. AZD120 treatment overcome resistance to α-PD-L1 mAb.
(A) The optimal cutoff percentage of CD36⁺PPARγ⁺ myeloid cells was estimated by a supervised machine learning method called Classification And Regression Tree (CART) analysis. (B) Therapy regimen schematic. (C-D) The frequency of CD206⁺Relmα⁺ M2 macrophages is shown in representative flow cytometry plots and quantified. (E-G) Human MDSCs were generated by culturing with tumor-conditioned medium and tested for suppressive activity (E), fatty acid uptake (F) and level of PPARγ (G). *p < 0.05. FMO = Fluorescence Minus One .

Supplemental Figure 8